ARTICLE IN PRESS

Inorganica Chimica Acta xxx (xxxx) xxx

Contents lists available at ScienceDirect

Inorganica Chimica Acta

journal homepage: www.elsevier.com/locate/ica

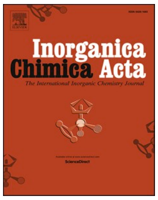

Research paper

Investigation on structurally different Cu(II) and Ni(II) complexes constructed from a novel pyridine-terminal salamo-like ligand

Ji-Fa Wang [a], Xin Xu [a], Ruo-Nan Bian [a], Wen-Kui Dong [a,*], Yu-Jie Ding [b,*]

[a] *School of Chemical and Biological Engineering, Lanzhou Jiaotong University, Lanzhou, Gansu 730070, China*
[b] *College of Biochemical Engineering, Anhui Polytechnic University, Wuhu 241000, China*

ARTICLE INFO

Keywords:
Salamo-like ligand
Complex
TGA analysis
Hirshfeld surface analysis
MOF

ABSTRACT

A novel structurally characterized salamo-like ligand H_2L contained double terminal pyridine groups was designed and synthesized. The single crystals of the Cu(II) and Ni(II) complexes are grown up through coordination of H_2L with Cu(II) and Ni(II) ions, respectively, determined as $[Cu(LH)]NO_3{\cdot}CH_3CH_2OH$ and $[\{Ni(L)\}_2]_n{\cdot}n3C_5H_5N{\cdot}nCH_3COCH_3$. The Cu(II) atom is located at the N_2O_2 cavity of the deprotonation ligand $(L)^{2-}$ moiety, but the N atoms of the terminal pyridine groups of the ligand $(L)^{2-}$ moiety is not involved in the coordination, and forms a four-coordinated twisted quadrilateral geometry. While the Ni(II) atom (Ni1 or Ni2) is sited in the N_2O_2 cavity of the deprotonation ligand $(L)^{2-}$ moiety and forms a plane, the terminal pyridine N atoms from the two adjacent [Ni(L)] moieties also coordinated with the Ni(II) atom in the axial positions to form a slightly distorted octahedral geometry with six-coordination. In the formation of MOFs, the benzene and pyridine rings of the ligand $(L)^{2-}$ moiety are rotated and create an angle, result to form a chiral MOFs using an achiral ligand $(L)^{2-}$ moiety. View of MOFs in the C direction, the Ni(II) complex has four different size of apertures in its structure, and presences a large amount of protonic hydrogen. Spectroscopic analyses of H_2L and its Cu(II) and Ni(II) complexes are performed using IR, UV–Vis and fluorescence spectroscopy. Compared with the Cu(II) complex, the Ni(II) complex has better thermal stability. The magnetic analyses were also carried out. Hirshfeld surfaces analyses are carried out to analyze various short-range interactions in H_2L and its Cu(II) complex.

1. Introduction

Salen-like compounds [1–7] are relatively common and versatile ligands in modern coordination chemistry, because they can provide stable N_2O_2 coordination sites, various metal complexes with novel structures can be obtained. In 2012, Feng *et al.* designed and synthesized a six-dentate salen-like ligand and obtained eight Ln(III) complexes, conducted detailed studies on their near-infrared luminescence and magnetic properties [8]. In 2014, Sandip *et al.* obtained three structurally different complexes by changing the solvent system and changing the ratio of the ligand with $Cu(NO_3)_2$. DFT calculations were used to reasonably explain their magnetic analysis [9]. In 2017, Kousik *et al.* synthesized three mononuclear Co(II) complexes, of which two complexes showed activities similar to phenoxazinone synthase [10]. In 2018, Angelica *et al.* designed and synthesized a salen-like ligand and its three transition metal complexes, and studied their spectral properties [11]. In addition, salen-like metal complexes also have potential application prospects in other aspects [12–18]. Due to the introduction of O atoms in the alkyl chain, salamo-like compounds [19–22] have better stability than salen-like compounds. Nearly decade, investigation on salamo-like ligands and their metal complexes [23,24] has been gradually deepened, and they have been found in ion recognition [25–34], antibacterial activity [35–38], catalysis [39], luminescence [40,41], magnetic [42] and other fields have good application prospects, the theoretical analyses were performed by DFT calculation [43] and Hirshfeld surface analysis [44–48].

Metal-organic frameworks (MOFs) [49–58] are attractive due to their regular pore channels with large porosity. In 2017, Guo *et al.* constructed a MOF using a pyridyl-terminal base ligand with auxiliary ligand, and applied to selectively separate Th(IV) from Ln(III) [59]. In 2018, on the basis of previous research, Ren *et al.* realized the replacement of metal ions in MOFs by introducing different metal ions, and obtained 6 isomorphic MOFs with excellent catalytic performances [60]. In 2019, Xia *et al.* developed a ligand containing pyridine group, and

---

* Corresponding authors.
E-mail addresses: dongwk@126.com (W.-K. Dong), yujieding123@163.com (Y.-J. Ding).

https://doi.org/10.1016/j.ica.2020.120095
Received 29 July 2020; Received in revised form 17 October 2020; Accepted 19 October 2020

Please cite this article as: Ji-Fa Wang, *Inorganica Chimica Acta*, https://doi.org/10.1016/j.ica.2020.120095

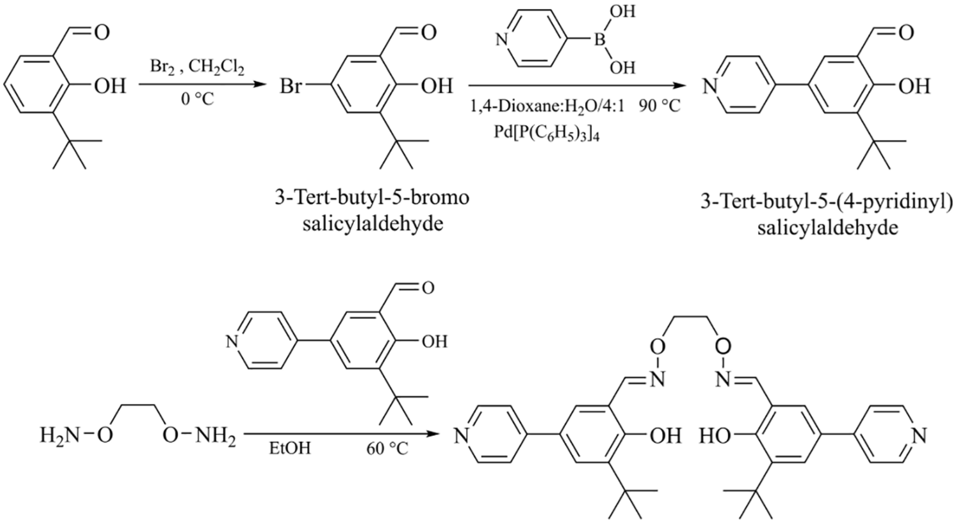

Scheme 1. Synthetic route to H_2L.

constructed three isomorphic MOFs via terephthalic acid and Cd(II), which were studied for gas adsorption and could be used as excellent catalysts [61].

In conclusion, the introduction of terminal pyridine groups into the ligand [59–61] can provide two potential coordination sites. When different metal ions are added to the ligand, it can cooperate with stable N_2O_2 coordination site to obtain structurally novel structures of complexes. Based on the in-depth study of salamo-like ligands, a novel salamo-like ligand H_2L contain double pyridine terminal groups was designed and synthesized, and obtained its crystal structure. By added different transition metal ions to the ligand H_2L, two complexes with large structural differences were formed, and novel MOF structure of the Ni(II) complex and mononuclear Cu(II) complex were obtained.

2. Experimental

2.1. Materials and physical measurements

Details of the materials and instruments for the experiment can be found in the Supporting Information.

2.2. Preparation of the ligand H_2L

The synthetic route to the ligand H_2L is shown in Scheme 1. According to the reference [58], 5-bromo-3-*tert*-butyl-salicylaldehyde and 3-*tert*-butyl-5-(4-pyridyl) salicylaldehyde have been synthesized. ^1H NMR spectra are shown in Figs. S1 and S2, respectively. 1,2-Bis(aminooxy)ethane was synthesized by reported reference [28]. 10 mL of anhydrous ethanol of 1,2-bis(aminooxy)ethane (0.21 g, 2.28 mmol) was added to 1.14 g (4.47 mmol) of 3-*tert*-butyl-5-(4-pyridyl) salicylaldehyde of 20 mL anhydrous ethanol solution. Reaction at 60 ℃ for 12 h, when the temperature was reduced to 20 °C, a white solid was precipitate. ^1H NMR spectrum of H_2L is shown in Fig. S3. Yield: 57.6% (744.24 mg). M. p.: 129–131 ℃. ^1H NMR (500 MHz, $CDCl_3$) δ 10.55 (s, 1H, –OH), 8.62 (d, $J = 6.0$ Hz, 2H, –ArH), 8.34 (s, 1H, –N=CH), 7.57 (s, 1H, –ArH), 7.43 (d, $J = 6.2$ Hz, 2H, –ArH), 7.29 (s, 1H, –ArH), 4.56 (s, 2H, $–CH_2$), 1.47 (s, 9H, $–CH_3$).

5.67 mg (0.01 mmol) of the ligand H_2L was dissolved in 1 mL of acetone, and then 4 mL of *n*-hexane was added. After the solution was mixed, the solution was filtered and sealed with tin foil. After stood for more than 1 week, the colourless block-shaped single crystal was obtained. Yield: 59%. Elemental analysis: *Anal.* calc. for H_2L ($C_{34}H_{38}N_4O_4$): C, 72.06; H, 6.76; N, 9.89. Found: C, 72.34; H, 6.71; N,

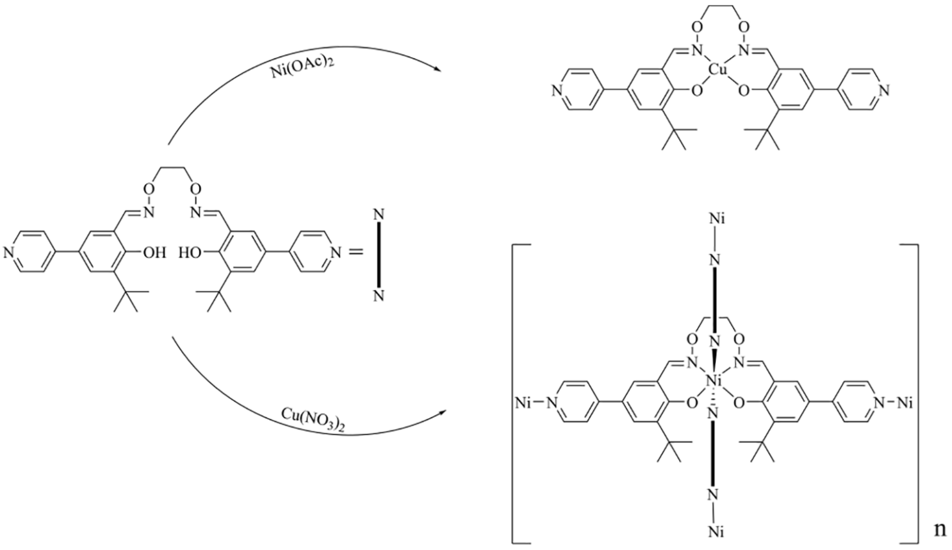

Scheme 2. Synthetic route to the Cu(II) and Ni(II) complexes.

Table 1
The crystal data and structure optimization of H_2L and its Cu(II) and Ni(II) complexes.

Compound	H_2L	The Cu(II) complex	The Ni(II) complex
Empirical formula	$C_{34}H_{38}N_4O_4$	$C_{36}H_{37}CuN_5O_8$	$C_{76}H_{83}N_9Ni_2O_9$
Molecular weight	566.68	737.29	1383.93
Crystal size (mm)	0.12 × 0.11 × 0.10	0.11 × 0.1 × 0.08	0.12 × 0.11 × 0.09
Habit	Block-shaped	Block-shaped	Block-shaped
Crystal system	Monoclinic	Triclinic	Tetragonal
Space group	$P2_1/C$	P-1	$P4_3$
Temperature/K	100.01(10)	100	100.01(10)
Wavelength (Å)	Mo Kα (λ = 0.71073)	Mo Kα (λ = 0.71073)	Mo Kα (λ = 0.71073)
a (Å)	6.1109(6)	7.3356(8)	21.0168(13)
b (Å)	10.6805(11)	15.399(2)	21.0168(13)
c (Å)	22.413(2)	16.432(2)	20.7903(19)
α (°)	90	92.948(10)	90
β (°)	92.528(8)	91.095(9)	90
γ (°)	90	100.092(10)	90
V (Å^3)	1461.4(3)	1824.3(4)	9183.2(14)
Z	2	2	4
D_{calc} (g · cm^{-3})	1.288	1.342	1.001
μ (mm^{-1})	0.085	0.655	0.459
F(000)	604.0	774.0	2920.0
2θ range for data collection (°)	4.226 to 58.978	4.966 to 49.996	4.344 to 50
Index ranges	$-6 \le h \le 8$, $-14 \le k \le 10$, $-29 \le l \le 25$	$-9 \le h \le 8$, $-18 \le k \le 18$, $-20 \le l \le 19$	$-24 \le h \le 20$, $-19 \le k \le 24$, $-24 \le l \le 24$
Reflections collected	6925	12,480	29,090
Independent reflections	3441 [R_{int} = 0.0462, R_{sigma} = 0.0875]	7168 [R_{int} = 0.0626, R_{sigma} = 0.1617]	14,467 [R_{int} = 0.0944, R_{sigma} = 0.1720]
Data/restraints/parameters	3441/0/266	7168/200/510	14467/336/879
GOF	1.107	1.086	0.982
Final R_1, wR_2 indices	0.0640,0.1153	0.0669, 0.1562	0.0718, 0.1349
R_1, wR_2 indices (all data)	0.1069,0.1386	0.1077, 0.1957	0.1116, 0.1580
Largest diff. peak and hole (e·Å^{-3})	0.25/−0.29	1.45/−0.65	0.59/−0.43

9.82.

2.3. Preparations of the Cu(II) and Ni(II) complexes

The synthetic route to the Cu (II) and Ni (II) complexes is depicted in Scheme 2.

The Cu(II) complex: 5.81 mg (0.01 mmol) H_2L was dissolved in 3 mL acetone, 2.42 mg (0.010 mmol) $Cu(NO_3)_2 \cdot 3H_2O$ was dissolved in 3 mL anhydrous ethanol. The dissolved anhydrous ethanol solution was added into the above acetone solution, the mixed solution immediately turned dark green, continuously stirred for 10 min, then filtered, sealed and remained still. After about 4 days, black block-shaped crystals suitable for X-ray diffraction were gained. Yield: 63%. Elemental analysis: *Anal.* calc. for $[Cu(LH)]NO_3 \cdot CH_3CH_2OH$ ($C_{36}H_{43}CuN_5O_8$) (%): C, 58.64; H, 5.88; N, 9.50; Cu, 8.62. Found (%): C, 59.71; H, 5.72; N, 9.41; Cu, 8.57.

The Ni(II) complex: 5.73 mg (0.01 mmol) H_2L was dissolved in 4 mL acetone, 2.47 mg (0.010 mmol) $Ni(CH_3COO)_2 \cdot 4H_2O$ was dissolved in 2 mL anhydrous ethanol. The dissolved anhydrous ethanol solution was added dropwise into the above-obtained acetone solution. The mixture immediately turned yellow green and became turbid during the stirring process, 5 drops of pyridine was added into the mixed solution, and the mixture became clear, stirred continuously for 35 min, then filtered and sealed. After about 1 week, yellow block-shaped single crystals suitable for X-ray diffraction were obtained. Yield: 54%. Although the single-crystal diffraction showed the product have the formula $[\{Ni(L)\}_2]_n \cdot nC_5H_5N \cdot nCH_3COCH_3$, the products can be best formulated as $[\{Ni(L)\}_2]_n \cdot n3C_5H_5N \cdot nCH_3COCH_3$ on the basis of microanalysis and TGA. Calcd for $C_{86}H_{93}Ni_2N_{11}O_9$ (%): C, 66.98; H, 6.08; N, 9.99; Ni, 7.61. Found (%): C, 67.73; H, 5.91; N, 9.82; Ni, 7.52.

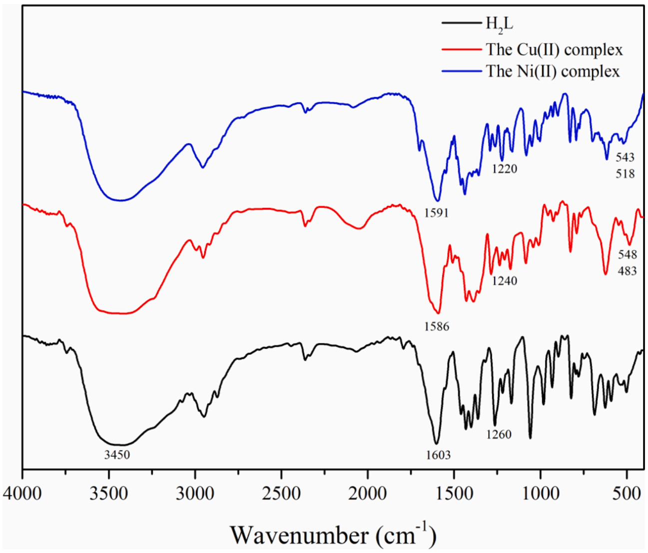

Fig. 1. IR spectra of H_2L and its Cu(II) and Ni(II) complexes.

2.4. X-ray structure determinations of H_2L and its Cu(II) and Cd(II) complexes

In the N_2 atmosphere, X-ray single crystal diffraction data of H_2L and its Cu(II) and Ni(II) complexes were collected under 100 K graphite monochromatic Mo-K_α radiation (λ = 0.71073 Å). The structures were solved by using the program (SHELXS-2015) [62,63], and Fourier difference techniques, and refined by full-matrix least-squares method on F^2. For other detailed information about crystal structure determination, please refer to the Supporting Information. The crystal data and structure optimization of H_2L and its Cu(II) and Ni(II) complexes are listed in Table 1.

3. Results and discussion

3.1. IR spectra analyses

As shown in Fig. 1, there are various absorption peaks in the range of 4000–400 cm^{-1} for the ligand H_2L and its Cu(II) and Ni (II) complexes. In the ligand H_2L, there is a large absorption peak at about 3450 cm^{-1}, which is caused by the stretching vibration of hydroxyl group in the ligand H_2L molecule, the strong absorption peak at about 1603 cm^{-1} is caused by the typical C═N stretching vibration, and the absorption peak at about 1260 cm^{-1} is the typical Ar-O stretching vibration. In the Cu(II) complex, there is a large absorption peak at about 3400 cm^{-1} due to the presence of water molecules in the manufactured of KBr lamination, while the typical C═N and Ar-O stretching vibrations appear at about 1586 and 1240 cm^{-1}, respectively, with significant low wavenumber displacements, indicate that coordination has taken place [64,65]. In addition, there are two medium absorption peaks at about 513 and 468 cm^{-1}, respectively, which are the absorption peaks of Cu–O and Cu–N bonds [66], show that Cu(II) ions are coordinated with the ligand H_2L. In the Ni(II) complex, a large absorption peak at about 3400 cm^{-1} due to the presence of water molecules in the manufactured of KBr lamination, while the typical C═N and Ar-O stretching vibrations appear at about

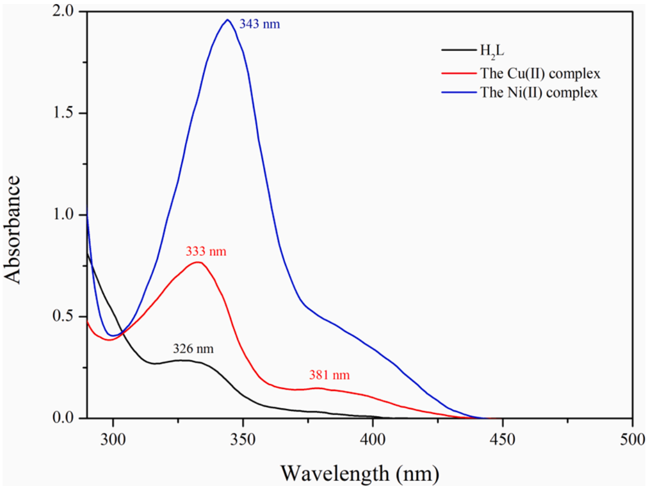

Fig. 2. UV–Vis spectra of H_2L and its Cu(II) and Ni(II) complexes.

1591 and 1220 cm^{-1}, respectively, with significant low wavenumber displacements, indicate that coordination has occurred. Besides, there are two medium absorption peaks at about 518 and 543 cm^{-1}, respectively, which are the absorption peaks of Ni-O and Ni-N bonds [66].

3.2. UV–Vis spectra analyses

The UV–Vis spectra of H_2L (DMF, 5×10^{-5} M) and its Cu(II) and Ni (II) complexes (DMF, 5×10^{-5} M) are shown in Fig. 2. In the absorption curve of the free ligand H_2L, there is a strong absorption peak at *ca.* 326 nm, which can be attributed to the π-π* transition of oxime group [67,68]. Compared with the free ligand H_2L, the absorption peak at *ca.* 326 nm in the Cu(II) complex has a red-shift to 333 nm (343 nm for the Ni(II) complex), this result may be due to the ligand to metal charge transition (LMCT) [69], which is consistent with the previous report, and similar to the ligand to metal charge transition in salen-like complexes [70]. In the Cu(II) complex, a new absorption peak at *ca.* 381 nm appears. The absorption peak at 381 nm is ultraviolet absorption, corresponding to a green color of the substance color (visual color), this is consistent with the observed phenomenon.

The titration curves of the Cu(II) and Ni(II) complexes are shown in Fig. 3. In Fig. 3a, with the addition of Cu^{2+} (1×10^{-3} M), the absorption peak intensity at *ca.* 326 nm increases gradually and the absorption peak shows an obvious red-shift. When 1 equiv. Cu^{2+} is add, the absorption peak has a red-shift to *ca.* 333 nm and the intensity reaches the maximum. After Cu^{2+} is continuously added, the absorption intensity at 333 nm does not changed any more. The results of titration show that the optimal ratio of H_2L to Cu^{2+} is 1:1. In Fig. 3b, with the addition of Ni^{2+} (1×10^{-3} M), a similar phenomenon appears, and the absorption peak has a red-shift to *ca.* 343 nm, and an isoabsorption point appears at *ca.* 304 nm. When 1 equiv. Ni^{2+} is add, the absorption intensity at *ca.* 343 nm will not increased any more, indicating that the optimal combination ratio of H_2L and Ni^{2+} is 1:1, which is consistent with the obtained single crystal structure by X-ray diffraction analysis.

3.3. Description of the crystal structures of H_2L and its Cu(II) and Ni(II) complexes

X-ray crystallographic analyses show that H_2L and its Cu(II) and Ni (II) complexes crystallize in different crystal systems, the selected bond lengths (Å) and angles (°) are listed in Table S1. Hydrogen bond and π···π stacking interactions are listed in Table S2.

3.3.1. Crystal structure of H_2L

As shown in Fig. 4, the ligand H_2L exists as a linear molecule in monoclinic system with the molecular formula of $C_{34}H_{38}N_4O_4$, and the whole molecule has a symmetrical structure.

As shown in Fig. S4, there are three pairs of obvious intramolecular hydrogen bonds (C(14)–H(14C)···O(1), C(15)–H(15A)···O(1) and O(1)–H(1)···N(1)) in the ligand H_2L molecule. In addition, there is a π···π stacking effect (Cg(1)···Cg(2)) between the two molecules, as shown in Fig. S5.

3.3.2. Crystal structure of the Cu(II) complex

As shown in Fig. 5, the Cu(II) complex is mononuclear. The complex consists of a completely deprotonation ligand $(L)^{2-}$ moiety and one Cu (II) atom. The Cu (II) atom (Cu1) is surrounded by two O atoms and two

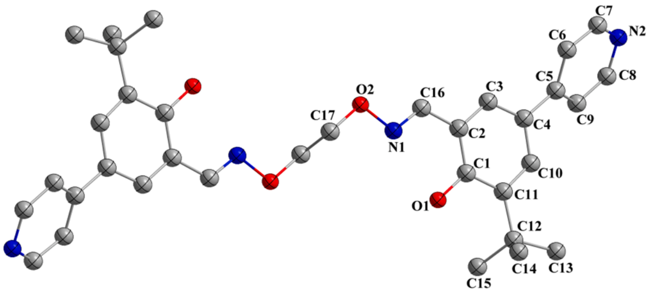

Fig. 4. The crystal structure of H_2L (hydrogen atoms are omitted for clarity).

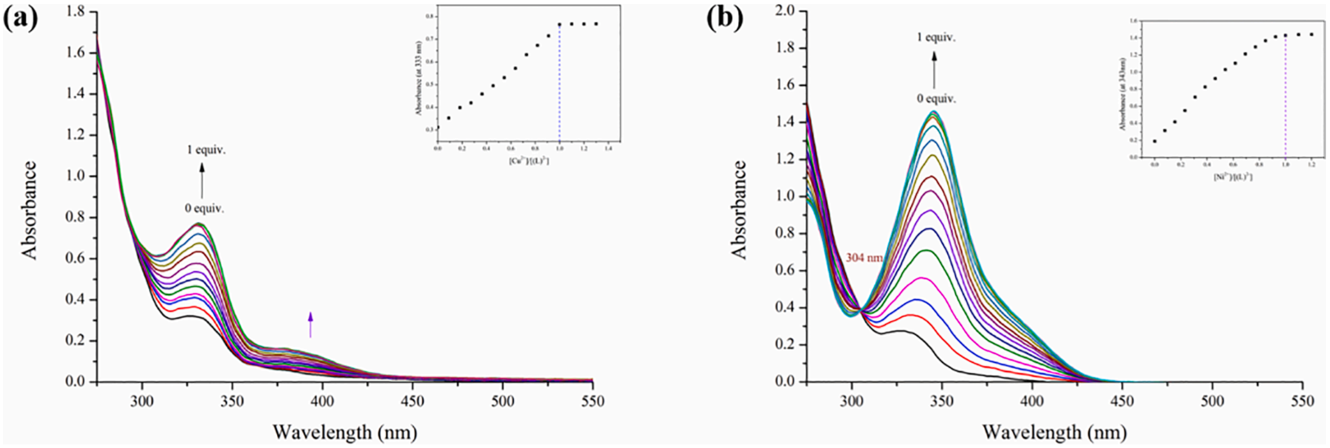

Fig. 3. (a) Continuous addition of Cu^{2+} (1×10^{-3} M) to H_2L (5×10^{-5} M) leads to a change in absorbance intensity; (b) Continuous addition of Ni^{2+} (1×10^{-3} M) to H_2L (5×10^{-5} M) leads to a change in absorbance intensity.

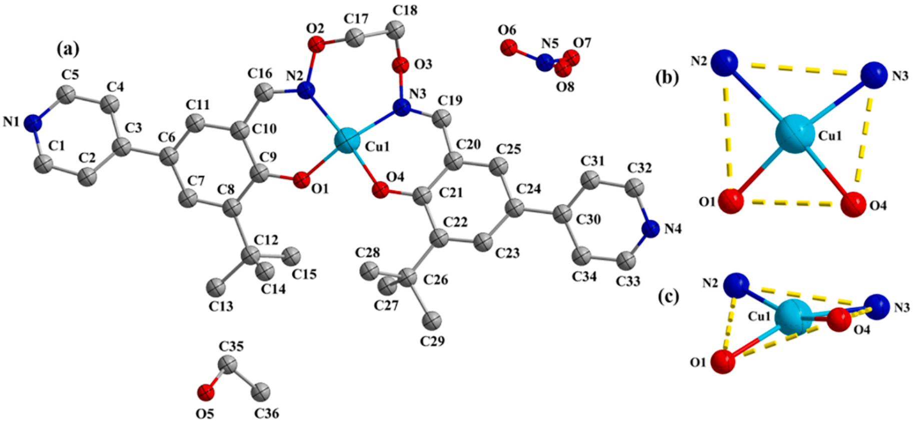

Fig. 5. (a) View of the molecular structure of the Cu(II) complex (hydrogen atoms are omitted for clarity). (b) and (c) Coordination polyhedron of the Cu(II) atom.

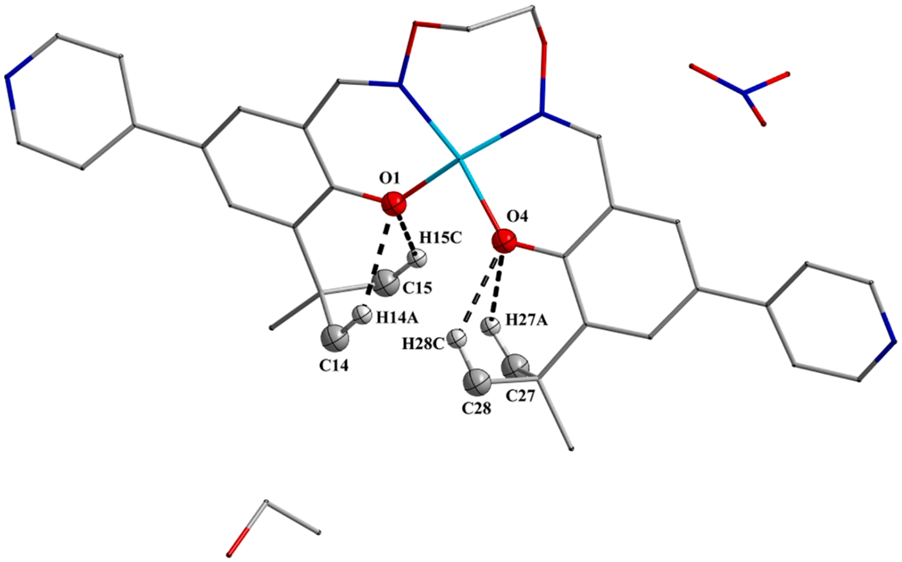

Fig. 6. The intramolecular hydrogen bonds of the Cu(II) complex.

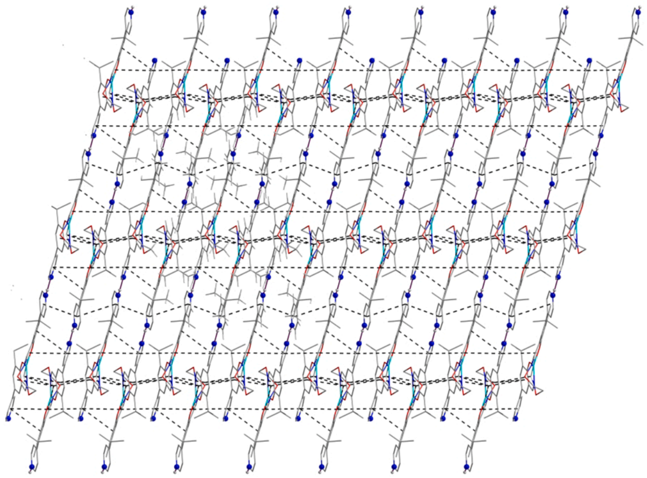

Fig. 7. 2-D supramolecular structure of the Cu(II) complex.

N atoms of the ligand $(L)^{2-}$ moiety, forming a slightly distorted planar quadrilateral geometry. Among them, two O atoms are phenolic oxygen atoms of the deprotonation ligand $(L)^{2-}$ moiety, and two N atoms are oxime N atoms of the deprotonation ligand $(L)^{2-}$ moiety.

In addition, there are four pairs of intramolecular hydrogen bonds (C(14)–H(14A)···O(1), C(15)–H(15C)···O(1), C(27)–H(27A)···O(4) and C(28)–H(28C)···O(4)) in the Cu(II) complex, as shown in Fig. 6.

There are also 4 kinds of π···π stacking interactions (Cg(6)···Cg(6), Cg(7)···Cg(2) , Cg(8)···Cg(5) and Cg(5)···Cg(4)) between adjacent molecules (Fig. S6a), and has one pairs of intermolecular hydrogen bond (N(2)–H(2)···N(4)) in the Cu(II) complex molecules (Fig. S6b). A 2-D supramolecular structure is obtain through the intermolecular hydrogen bond and the π···π stacking interactions (Fig. 7).

3.3.3. *Crystal structure of the Ni(II) complex*

In the Ni(II) complex (Fig. 8), the Ni(II) atom (Ni1 or Ni2) is surrounded by two O atoms (O1, O4 or O5, O8) and four N atoms (N1, N2, N6, N8 or N4, N5, N3, N7), which two O atoms (O1, O4 or O5, O8) and two N atoms (N1, N2 or N4, N5) are provided by the N_2O_2 cavity of the deprotonation ligand $(L)^{2-}$ moiety to form a plane, while the other two N atoms (N6, N8 or N3, N7) are come from the terminal pyridine groups of adjacent two [Ni(L)] units, and coordinated with the Ni(II) atoms in the axial positions to form a slightly distorted *hexa*-coordinated octahedral geometrical configuration. There are soft alkyl chains in salamo-like ligands, which may lead to a certain distortion of the plane formed by N_2O_2 cavity, lead to the existence of two six-coordinated Ni(II) atoms in the smallest symmetry unit, but the coordination modes and

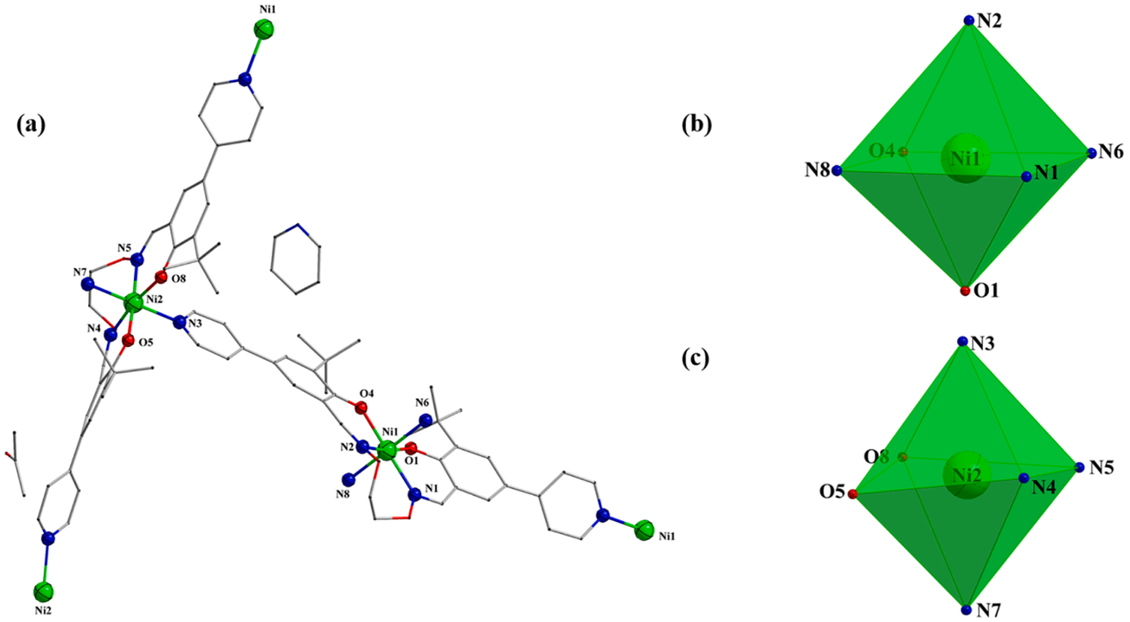

Fig. 8. (a) View of the molecular structure of the Ni(II) complex (hydrogen atoms are omitted for clarity). (b) and (c) Coordination polyhedrons of Ni(II) atoms.

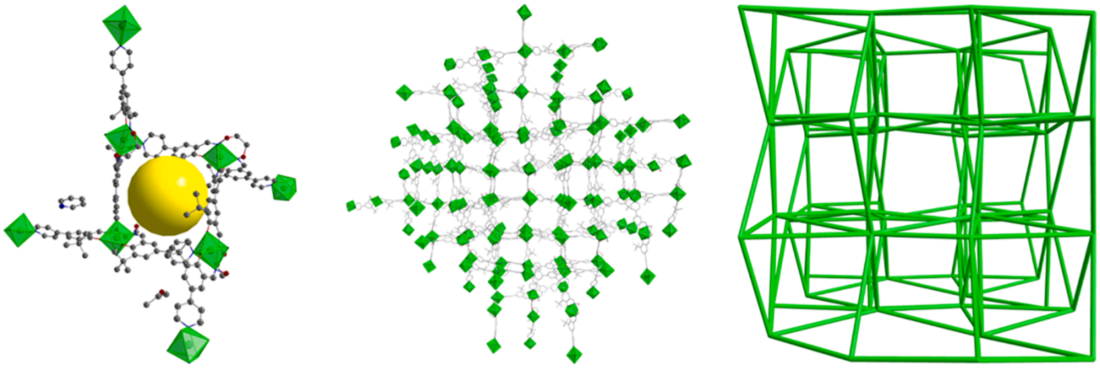

Fig. 9. Three-dimensional topology of the Ni(II) complex.

geometries are similar. The coordination modes of the Ni(II) atoms lead to the self-assembly of three-dimensional metal organic framework (MOFs) with Ni(II) atom as the node, and regular channels can be seen in the C direction.

On account of the benzene ring and pyridine ring in the ligand H_2L is linked by a single bond, they can rotate freely. As shown in Fig. S7, there are 4 different dihedral angles in the smallest symmetric unit, which leads to the possibility of many more combinations of the ligand H_2L and Ni(II) atoms in the formation of MOFs. Due to a certain distortion between the benzene ring and the pyridine ring that leads to form a MOFs possessing a chiral space group while used the non-chiral ligand H_2L. In Fig. S8, four apertures of different sizes are observed in the C direction. Fig. 9 is a 3D topological diagram of the Ni(II) complex.

In addition, there are 14 pairs of obvious intramolecular hydrogen bonds (C(4)–H(4B)···N(8), C(15)–H(15)···N(5), C(20)–H(20B)···N(7), C(54)–H(54A)···O(4), C(31)–H(231)···O(4), C(34)–H(34C)···O(8), C(35)–H(35A)···O(8), C(42)–H(42C)···O(5), C(43)–H(43A)···O(5), C(61)–H(61A)···O(1), C(48)–H(48)···O(8), C(50)–H(50)···O(5), C(62)–H(62C)···O(1) and C(53)–H(53C)···O(4)) in the Ni(II) complex (Fig. 10), and two pairs of intermolecular hydrogen bonds (C(29)–H(29)···O(7) and C(46)–H(46)···O(9)) between the Ni(II) complex molecules and between the Ni(II) complex and the solvent acetone molecule (Fig. 11).

3.4. *Hirshfeld surfaces analyses*

Hirshfeld surfaces analyses of H_2L and its Cu(II) complex are carried out. In Fig. 12, the Hirshfeld surfaces of H_2L and its Cu(II) complex are mapped to dnorm, shape index and curvature. Take H_2L as an example, in the map of dnorm, the red region represents the O···H/H···O interaction in H_2L, the darker the color, the stronger the interaction; the other regions represent other short-range interactions. In the two-dimensional fingerprint, gray represents the whole fingerprint, while the blue area represents the proportion of each short-range effect.

Taking the O···H/H···O interactions as an example, the O···H interaction is mainly concentrated in the peak position at the bottom right of the fingerprint, while the H···O interaction is mainly concentrated in the peak position at the top left of the fingerprint. The proportion of O···H/H···O interactions is 6.5%. The proportions of C···H/H···C, N···H/H···N and H···H interactions in H_2L are 25.7%, 10.2% and 55.2%, respectively. Therefore, H—H interaction is the main interaction in H_2L. In the Cu(II) complex, the proportions of O···H/H···O, C···H/H···C, N···H/H···N and H···H interactions are 5.8%, 7.2%, 2.2% and 68.6%, respectively. Therefore, H···H interaction is the main interaction in the Cu(II) complex.

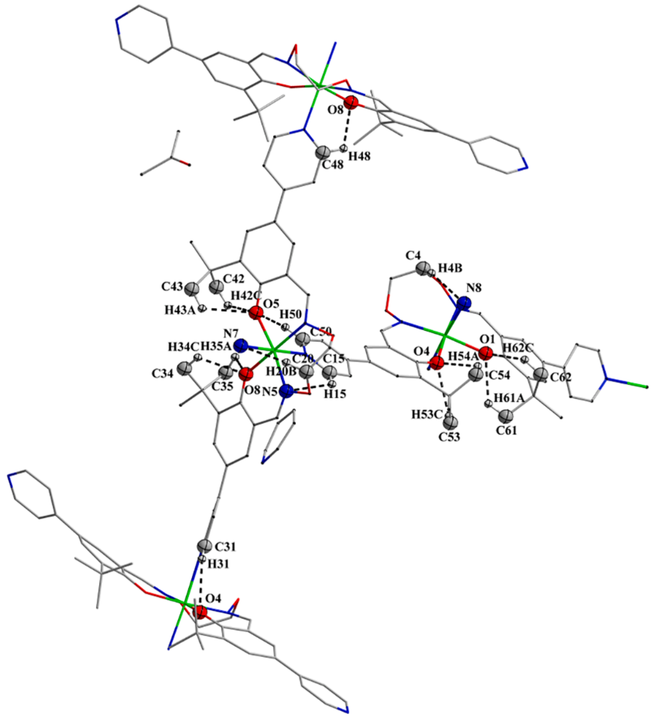

Fig. 10. The intramolecular hydrogen bonds of the Ni(II) complex.

3.5. TGA analyses

Weigh out 5 mg of the Cu(II) and Ni(II) complexes respectively, control the heating rate at 10 ℃/min, the thermal stabilities of the two complexes were measured using thermogravimetric analyzer. As shown in Fig. 13, the weight loss of the Cu(II) complex is mainly divided into two stages. The weight loss is 25.7% in the range of 35–254 °C, and the weight loss of the crystallized ethanol molecule and one nitrate group in the Cu(II) complex is calculated as 14.7%, so this result should be a weight loss due to the loss of the crystallized solvent molecule and the nitrate group in the Cu(II) complex. In the range of 303–425 ℃, the weight loss is caused by the decomposition of the main framework of the Cu(II) complex. After 500 ℃, the weight will not be lost, the remaining weight was 11.6%, and the theoretical analysis of CuO was 10.9%. The two values are close, so it is inferred that the Cu(II) complex will generate its oxide after being heated at 500 ℃.

The weight loss of the Ni(II) complex can be divided into two stages. The weight loss is 25.3% in the range of 43–264 °C, and the weight loss of the crystallized acetone and three crystallized pyridine molecules in the Ni(II) complex is calculated as 19.2%, so this should be a weight loss due to the loss of solvent molecules in the Ni(II) complex. After 550 ℃, the weight will not be lost, the remaining weight was 10.01%, and the theoretical analysis of NiO was 9.7%. The two values are close, so it can be concluded that the Ni(II) complex will generate its oxide after being heated at 550 ℃. Thermogravimetric analyses show that the two complexes could withstand the high temperature of more than 300 ℃, while the Ni(II) complex could withstand the high temperature of more than 360 ℃ and keep the structure intact, indicating that the Ni(II) complex has better thermal stability compared with the Cu(II) complex.

3.6. Fluorescence properties

With 350 nm as excitation wavelength and 10 / 20 nm as slit, the ligand H_2L and its Cu(II) and Ni(II) complexes use anhydrous ethanol as solvent. The fluorescence spectra of H_2L (5×10^{-5} M) and its Cu(II) and Ni(II) complexes (5×10^{-5} M) are shown in Fig. 14.

The ligand H_2L has an emission peak at approximately 466 nm, which may be due to the π-π* transition within the ligand [71]. While the emission peaks of the Cu(II) and Ni(II) complexes at 466 nm disappear significantly, decrease of fluorescence intensity in the Cu(II) and Ni(II) complexes may be due to the introduction of the Cu(II) and Ni (II) ions into the ligand [72].

The titration curves of the Cu(II) and Ni(II) complexes are shown in Fig. 15. In Fig. 15a, with the addition of Cu^{2+} (1×10^{-3} M), the fluorescence intensity at appromately 466 nm decreases gradually. When 1 equivalent Cu^{2+} is add, the emission peak at 466 nm is reduced to the minimum. In the wake of continued to add Cu^{2+}, the fluorescence intensity at 466 nm will not change any more. The titration results show that the optimal binding ratio of the ligand H_2L to Cu^{2+} is 1:1, which is consistent with the single crystal structure obtained by X-ray diffraction analysis. In Fig. 15b, a similar phenomenon occurs with the addition of Ni^{2+} (1×10^{-3} M), when 1 equivalent Ni^{2+} is add, the fluorescence intensity at 466 nm will not decrease any more, indicating that the optimal binding ratio of the ligand H_2L to Cd^{2+} is 1:1.

3.7. Magnetic analyses

The variable temperature magnetic susceptibility data of the Cu(II) and Ni(II) complexes were measured under an external magnetic field of 10,000 Oe.

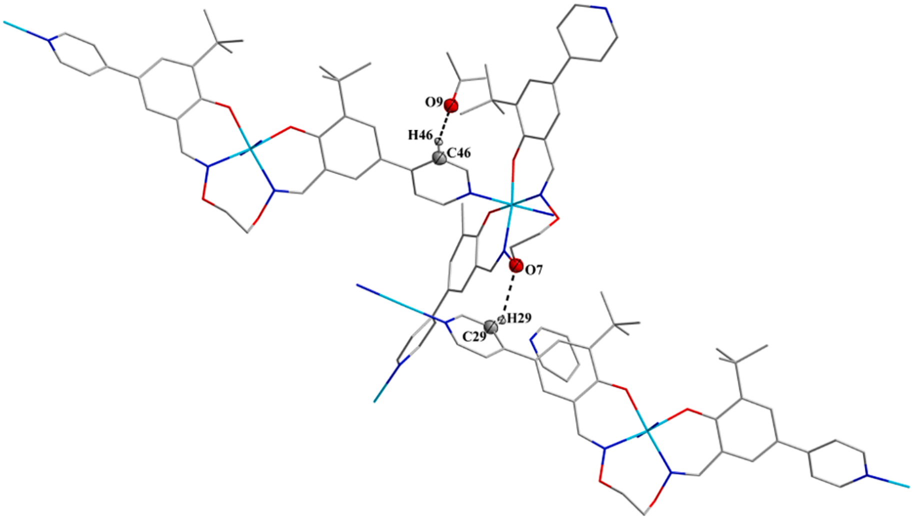

Fig. 11. The intermolecular hydrogen bonds of the Ni(II) complex.

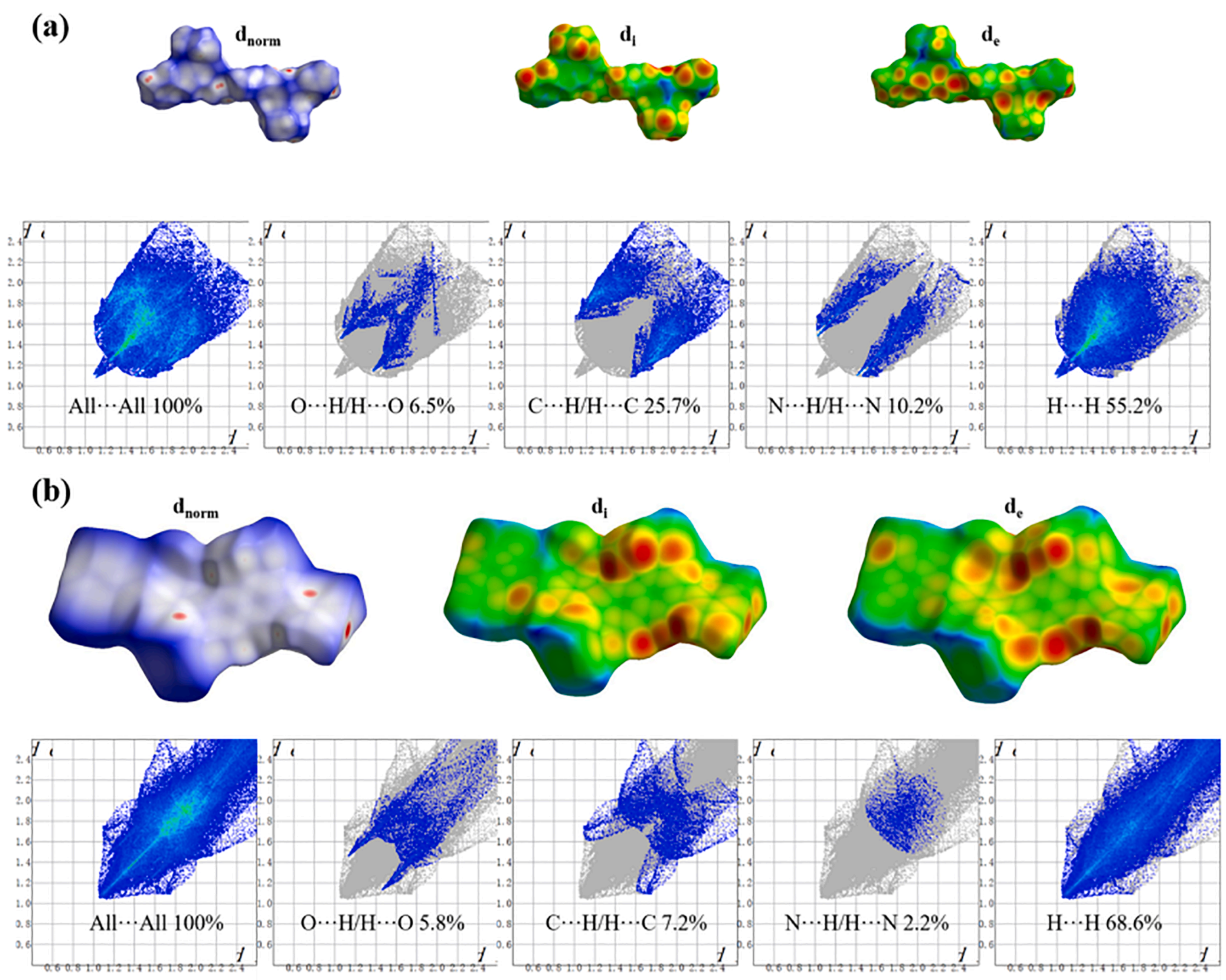

Fig. 12. (a) Hirshfeld surface analysis mapping and various 2D fingerprints of H_2L. (b) Hirshfeld surface analysis mapping and various 2D fingerprints of the Cu (II) complex.

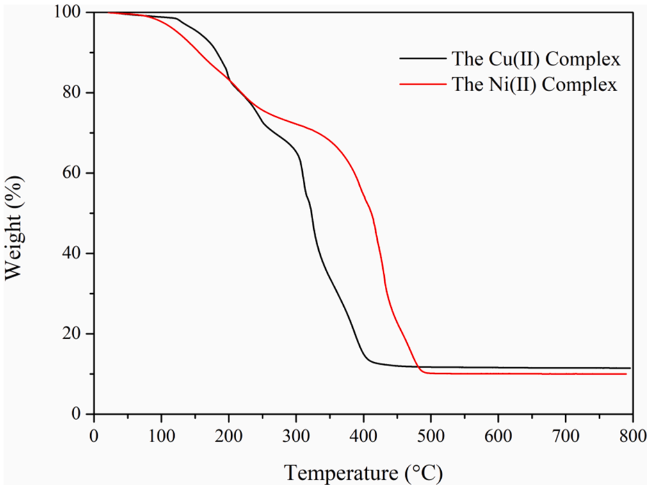

Fig. 13. TGA curves of the Cu(II) and Ni(II) complexes.

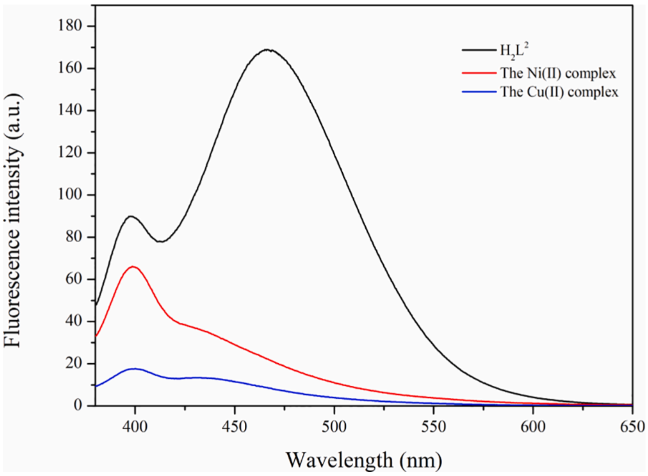

Fig. 14. Fluorescence spectra of H_2L and its Cu(II) and Ni(II) complexes.

The variable temperature magnetic susceptibility of the Cu(II) complex is shown in Fig. 16. At 300 K, the $\chi_M T$ value of the mononuclear Cu(II) complex is 0.379 cm^3 K mol^{-1}, the $\chi_M T$ value decreases with the decrease of the temperature, and the decreasing speed begins to increase when the temperature drops to about 10 K. When the temperature drops to about 2 K, the $\chi_M T$ value decreases to 0.334 cm^3 K mol^{-1}, which

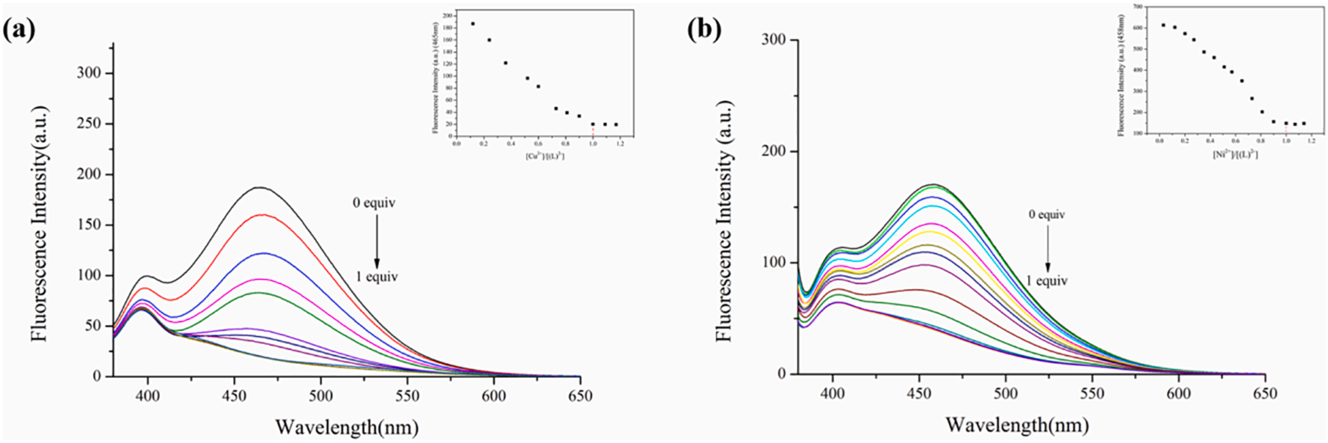

Fig. 15. (a) Continuous addition of Cu^{2+} (1×10^{-3} M) to H_2L (5×10^{-5} M) leads to a change in fluorescence intensity; (b) Continuous addition of Ni^{2+} (1×10^{-3} M) to H_2L (5×10^{-5} M) leads to a change in fluorescence intensity.

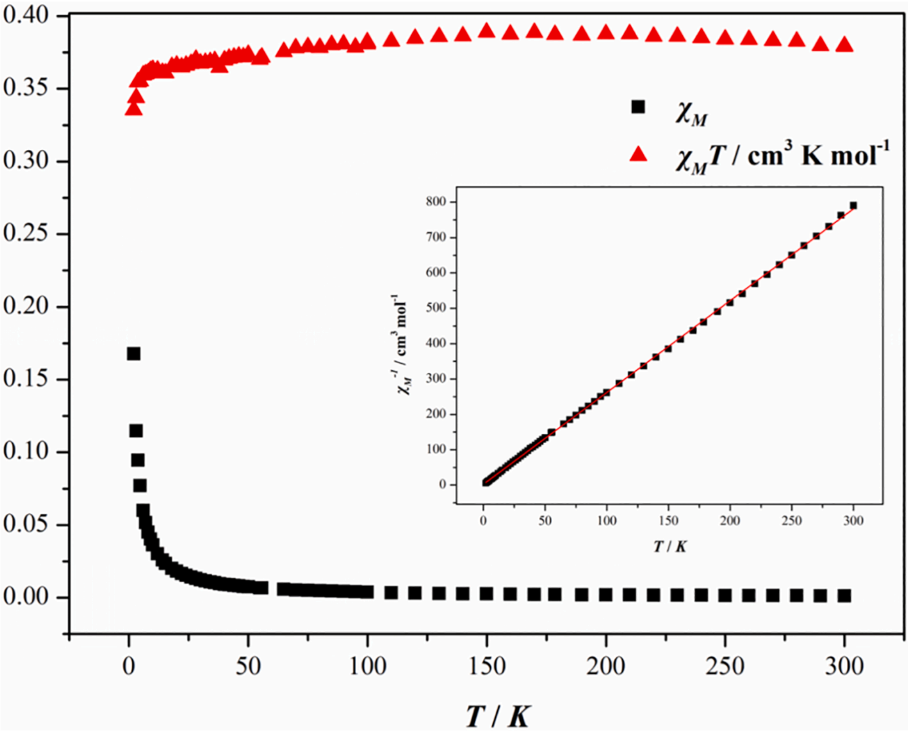

Fig. 16. $\chi_M T$ / T and χ_M^{-1} / T curves of the Cu(II) complex (the red solid line is the fitted curve). (For interpretation of the references to color in this figure legend, the reader is referred to the web version of this article.)

indicates that there is a weak antiferromagnetic effect in the Cu(II) complex. In the range of 2 ~ 300 K, the Curie-Weiss theorem ($\chi_M = C/(T–\theta)$) is used to fit the obtained data reasonably, and the fitting constant $C = 0.385$ cm^3 K mol^{-1} and Weiss constant $\theta = -0.899$ K are calculated. The Weiss constant is negative, and according to the change trend of the molar susceptibility of the Cu(II) complex in the temperature range of 2 ~ 300 k, there is a weak antiferromagnetic effect in the Cu(II) complex.

The variable temperature magnetic susceptibility of the Ni(II) complex is shown in Fig. 17. At 300 K, the $\chi_M T$ value of the Ni(II) complex is 1.319 cm^3 K mol^{-1}, the $\chi_M T$ value increases with the decrease of temperature. When the temperature decreases to about 30 K, the $\chi_M T$ value reaches the maximum value of 1.564 cm^3 K mol^{-1}, and then decreases with the decrease of temperature. When the temperature decreases to 2 K, the $\chi_M T$ value decreases to 0.980 cm^3 K mol^{-1}, which indicates that there is weak ferromagnetism in the Ni(II) complex. In the range of 2 ~ 300 K, the Curie-Weiss theorem ($\chi_M = C/(T\text{-}\theta)$) is used to fit the obtained data reasonably, and the fitting constant $C = 1.365$ cm^3 K mol^{-1} and Weiss constant $\theta = 5.056$ K are also calculated. The Weiss constant is positive. According to the change trend of the molar susceptibility of the Ni(II) complex in the temperature range of 2 ~ 300 K, there is weak ferromagnetism in the Ni(II) complex.

4. Conclusion

A novel salamo-like ligand containing double terminal pyridine groups was synthesized and characterized structurally. The single crystals of H_2L were obtained by natural volatile solvent method. Two novel Cu(II) and Ni (II) complexes were obtained by adding Cu(II) and Ni (II) ions into H_2L. Among them, the Cu(II) complex is a common mononuclear complex, which forms a one-dimensional supramolecular

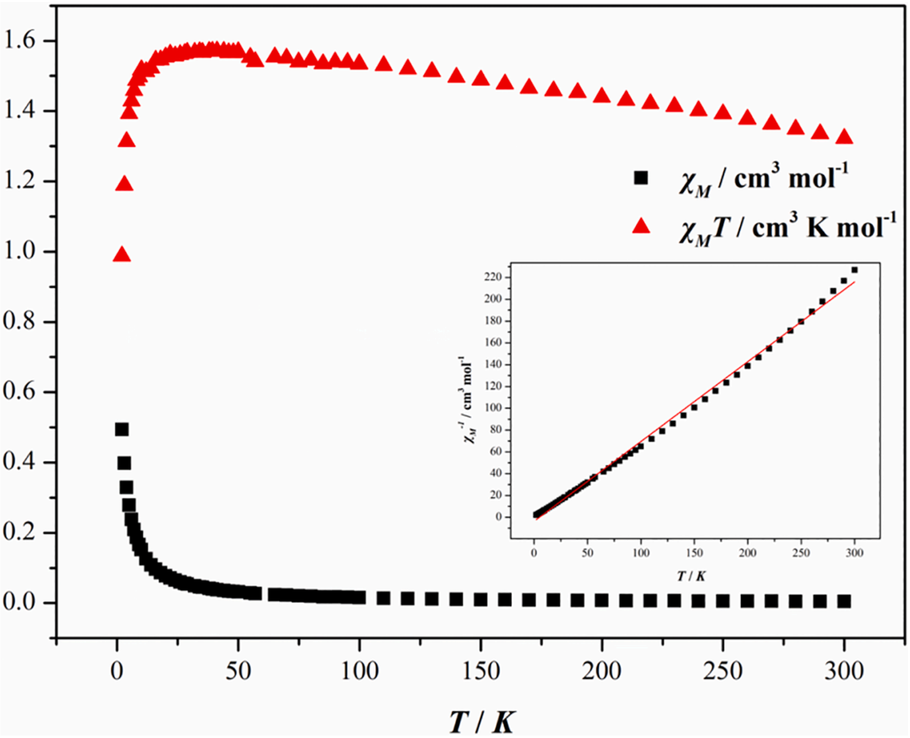

Fig. 17. $\chi_M T$ / T and χ_M^{-1} / T curves of the Ni(II) complex (the red solid line is the fitted curve). (For interpretation of the references to color in this figure legend, the reader is referred to the web version of this article.)

structure through intermolecular hydrogen bonds; while a metal–organic framework (MOFs) with regular pore size is self-assembled via the coordination of the Ni(II) ion with H_2L. Fluorescence and UV–Vis analyses of the two obtained complexes are carried out, and TGA analysis determines that the two complexes had better thermal stabilities. By Hirshfeld surface analysis, a theoretical analysis of the presence of various interactions in H_2L and its Cu(II) complex are carried out. The results of magnetic analyses show that there is weak antiferromagnetic interaction in the Cu(II) complex and weak ferromagnetic interaction in the Ni(II) complex.

Declaration of Competing Interest

The authors declare that they have no known competing financial interests or personal relationships that could have appeared to influence the work reported in this paper.

Acknowledgements

This work was supported by the National Natural Science Foundation of China (21968032), Special Funds for Discipline Construction of Gansu Agricultural University (LXYXK201801) and the Program for Excellent Team of Scientific Research in Lanzhou Jiaotong University (201706), which are gratefully acknowledged.

Appendix A. Supplementary data

Supplementary data to this article can be found online at https://doi.org/10.1016/j.ica.2020.120095.

References

[1] T. Nakamura, S. Tsukuda, T. Nabeshima, J. Am. Chem. Soc. 141 (2018) 6462–6467.
[2] Y. Sakata, S. Chiba, M. Miyashita, T. Nabeshima, S. Akine, Chem. Eur. J. 25 (2019) 2962–2966.
[3] A. Sumiyoshi, Y. Chiba, R. Matsuoka, T. Noda, T. Nabeshima, Dalton Trans. 48 (2019) 13169–13175.
[4] C.H. Ryu, S.W. Kwak, H.W. Lee, J.H. Lee, H. Hwang, M. Kim, Y. Chung, Y. Kim, M. H. Park, K.M. Lee, Inorg. Chem. 58 (2019) 12358–12364.
[5] S. Akine, S. Piao, M. Miyashita, T. Nabeshima, Tetrahedron Lett. 54 (2013) 6541–6544.
[6] T. Nabeshima, M. Yamamura, Pure Appl. Chem. 85 (2013) 763–776.
[7] S. Akine, Z. Varadi, T. Nabeshima, Eur. J. Inorg. Chem. 35 (2013) 5987–5998.
[8] W.X. Feng, Y. Zhang, Z. Zhang, X.Q. Lü, H. Liu, G.X. Shi, D. Zou, J.R. Song, D. D. Fan, W.K. Wong, R.A. Jones, Inorg. Chem. 51 (2012) 11377–11386.
[9] S. Mukherjee, P.S. Mukherjee, Cryst. Growth Des. 14 (2014) 4177–4186.
[10] K. Ghosh, K. Harms, S. Chattopadhyay, Polyhedron 123 (2017) 162–175.
[11] A. Vlad, M. Avadanei, S. Shova, M. Cazacu, M.F. Zaltariov, Polyhedron 146 (2018) 129–135.
[12] J.G. Duan, Y. Li, Y. Pan, N. Behera, W. Jin, Coord. Chem. Rev. 395 (2019) 25–45.
[13] C. Lochenie, S. Schlamp, A.P. Railliet, K. Robeyns, B. Weber, Y. Garcia, CrystEngComm 16 (2014) 6213–6218.
[14] J.G. Duan, W.Q. Jin, S. Kitagawa, Coord. Chem. Rev. 332 (2017) 48–74.
[15] S.G. Dogaheh, H. Khanmohammadi, E.C. Sañudo, Polyhedron 133 (2017) 48–53.
[16] J.G. Duan, M. Higuchi, J. Zheng, S.I. Noro, I.Y. Chang, K. Hyeon-Deuk, S. Mathew, S. Kusaka, E. Sivaniah, R. Matsuda, S. Sakaki, S. Kitagawa, J. Am. Chem. Soc. 139 (2017) 11576–11583.
[17] M. Azam, S.I. Al-Resayes, A. Trzesowska-Kruszynska, R. Kruszynski, P. Kumar, S. L. Jain, Polyhedron 124 (2017) 177–183.
[18] Y. Yue, G.F. Hou, X. Yao, G.M. Li, Polyhedron 129 (2017) 157–163.
[19] Y.Q. Pan, Y. Zhang, M. Yu, Y. Zhang, L. Wang, Appl. Organomet. Chem. 34 (2020) e5441.
[20] L.W. Zhang, Y. Zhang, Y.F. Cui, M. Yu, W.K. Dong, Inorg. Chim. Acta 506 (2020) 119534.
[21] S.Z. Zhang, J. Chang, H.J. Zhang, Y.X. Sun, Y. Wu, Y.B. Wang, Chin. J. Inorg. Chem. 36 (2020) 503–514.
[22] Q.P. Kang, X.Y. Li, Z.L. Wei, Y. Zhang, W.K. Dong, Polyhedron 165 (2019) 38–50.
[23] L.Z. Liu, M. Yu, X.Y. Li, Q.P. Kang, W.K. Dong, Chin. J. Inorg. Chem. 35 (2019) 1283–1294.
[24] Y. Zhang, L.Z. Liu, Y.D. Peng, N. Li, W.K. Dong, Transit. Met. Chem. 44 (2019) 627–639.
[25] Y.Q. Pan, X. Xu, Y. Zhang, Y. Zhang, W.K. Dong, Spectrochim. Acta A 229 (2020) 117927.
[26] Z.L. Wei, L. Wang, J.F. Wang, W.T. Guo, Y. Zhang, W.K. Dong, Spectrochim. Acta A 228 (2020) 117775.
[27] L. Wang, Z.L. Wei, Z.Z. Chen, C. Liu, W.K. Dong, Y.J. Ding, Microchem. J. 155 (2020) 104801.
[28] C. Liu, Z.L. Wei, H.R. Mu, W.K. Dong, Y.J. Ding, J. Photochem. Photobio. A 397 (2020) 112569.
[29] L. Wang, Z.L. Wei, C. Liu, W.K. Dong, J.X. Ru, Spectrochim. Acta A 239 (2020) 118496.

[30] H.R. Mu, M. Yu, L. Wang, Y. Zhang, Y.J. Ding, Phosphorus Sulfur Silicon Relat. Elem. 195 (2020) 730–739.
[31] L.Z. Liu, L. Wang, M. Yu, Q. Zhao, Y. Zhang, Y.X. Sun, W.K. Dong, Spectrochim. Acta A 222 (2019) 117209.
[32] H.R. Mu, X.X. An, C. Liu, Y. Zhang, W.K. Dong, J. Struct. Chem. 61 (7) (2020) 1218–1229.
[33] Y.D. Peng, Y. Zhang, Y.L. Jiang, Z.L. Ren, F. Wang, L. Wang, J. Fluores. 30 (2020) 1049–1061.
[34] Z.L. Wei, L. Wang, S.Z. Guo, Y. Zhang, W.K. Dong, RSC Adv. 9 (2019) 41298.
[35] C. Liu, X.X. An, Y.F. Cui, K.F. Xie, W.K. Dong, Appl. Organomet. Chem. 34 (2020) e5272.
[36] Y.F. Cui, Y. Zhang, K.F. Xie, W.K. Dong, Crystals 9 (2019) 596.
[37] Y. Zhang, M. Yu, Y.Q. Pan, Y. Zhang, L. Xu, X.Y. Dong, Appl. Organomet. Chem. 34 (2020) e5442.
[38] L. Wang, Y.Q. Pan, J.F. Wang, Y. Zhang, Y.J. Ding, J. Photochem. Photobio. A 400 (2020) 112719.
[39] X.Y. Li, Q.P. Kang, C. Liu, Y. Zhang, W.K. Dong, New J. Chem. 43 (2019) 4605–4619.
[40] Q. Zhao, X.X. An, L.Z. Liu, W.K. Dong, Inorg. Chim. Acta 490 (2019) 6–15.
[41] Q.P. Kang, X.Y. Li, L. Wang, Y. Zhang, W.K. Dong, Appl. Organomet. Chem. 33 (2019) e5013.
[42] R.N. Bian, J.F. Wang, Y.J. Li, Y. Zhang, W.K. Dong, J. Photochem. Photobiol. A. 400 (2020) 112829.
[43] J. Chang, S.Z. Zhang, Y. Wu, H.J. Zhang, Y.X. Sun, Transit. Met. Chem. 45 (2020) 279–293.
[44] M. Yu, Y. Zhang, Y.Q. Pan, L. Wang, Inorg. Chim. Acta 509 (2020) 119701.
[45] X.X. An, Q. Zhao, H.R. Mu, W.K. Dong, Crystals 9 (2019) 101.
[46] Y.X. Sun, Y.Q. Pan, X. Xu, Y. Zhang, Crystals 9 (2019) 607.
[47] L. Xu, M. Yu, L.H. Li, J.C. Ma, W.K. Dong, J. Struct. Chem. 60 (2019) 1358.
[48] M. Yu, H.R. Mu, L.Z. Liu, N. Li, Y. Bai, X.Y. Dong, Chin. J. Inorg. Chem. 35 (2019) 1109.
[49] X. Han, Q.C. Xia, J.J. Huang, Y. Liu, C.X. Tan, Y. Cui, J. Am. Chem. Soc. 139 (2017) 8693–8697.
[50] C.F. Zhu, G.Z. Yuan, X. Chen, Z.W. Yang, Y. Cui, J. Am. Chem. Soc. 134 (2012) 8058–8061.
[51] A.M. Shultz, A.A. Sarjeant, O.K. Farha, J.T. Hupp, S.T. Nguyen, J. Am. Chem. Soc. 133 (2011) 13252–13255.
[52] G.A.E. Oxford, R.Q. Snurr, L.J. Broadbelt, Ind. Eng. Chem. Res. 49 (2010) 10965–10973.
[53] Y.B. Huang, T.F. Liu, J.X. Lin, J. Lu, Z.J. Lin, R. Cao, Inorg. Chem. 50 (2011) 2191–2198.
[54] F.J. Song, C. Wang, J.M. Falkowski, L.Q. Ma, W.B. Lin, J. Am. Chem. Soc. 132 (2010) 15390–15398.
[55] X.B. Xi, Y. Fang, T.W. Dong, Y. Cui, Angew. Chem. 123 (2011) 1186–1190.
[56] T.U. Yoon, M.J. Kim, A.R. Kima, J.H. Kang, D. Jia, Y.S. Bae, J. Ind. Eng. Chem. 87 (2020) 102–109.
[57] Y.Y. Li, X.M. Li, Y.T. Pan, X.Y. Xu, Y.Z. Song, R.Z. Yang, J. Hazard. Mater. 395 (2020) 122604.
[58] S.B. Xia, Y.X. Yan, W.J. Huang, R.M. Yang, H.B. Suo, J.M. L, F.X. Cheng, J.J. Liu, J. Power Sources 464 (2020) 228247.
[59] X.G. Guo, S. Qiu, X.T. Chen, Y. Gong, X.Q. Sun, Inorg. Chem. 6 (2017) 12357–12361.
[60] J.W. Li, Y.M. Fan, Y.W. Ren, J.H. Liao, C.R. Qi, H.F. Jiang, Inorg. Chem. 57 (2018) 1203–1212.
[61] Q.C. Xia, C. Yuan, Y.X. Li, Y. Cui, Chem. Comm. 55 (2019) 9136–9139.
[62] W.I. Madison, SAINT-Plus, Bruker Analytical X-ray System, Billerica, Bruker, MA, USA, 1999.
[63] G.M. Sheldrick, SADABS, Program for Empirical Absorption Correction of Area Detector Data, University of Gottingen, Gottingen, Germany, 1996.
[64] Y. Zhang, Y.Q. Pan, M. Yu, X. Xu, W.K. Dong, Appl. Organomet. Chem. 33 (2019) e5240.
[65] X.X. An, Z.Z. Chen, H.R. Mu, L. Zhao, Inorg. Chim. Acta 511 (2020) 119823.
[66] A. Majumder, G.M. Rosair, A. Mallick, N. Chattopadhyay, S. Mitra, Polyhedron 25 (2006) 1753.
[67] S. Akine, Y. Morita, F. Utsuno, T. Nabeshima, Inorg. Chem. 48 (2009) 10670–10678.
[68] X. Xu, R.N. Bian, S.Z. Guo, W.K. Dong, Y.J. Ding, Inorg. Chim. Acta 513 (2020) 119945.
[69] Y. Zhang, Y.J. Li, S.Z. Guo, T. Fu, L. Zhao, Transit. Met. Chem. 45 (2020) 485–492.
[70] L. Wang, Z.L. Wei, M. Yu, Y.Q. Pan, Y. Zhang, W.K. Dong, Chin. J. Inorg. Chem. 35 (2019) 1791.
[71] X.X. An, C. Liu, Z.Z. Chen, K.F. Xie, W.K. Dong, Crystals 9 (2019) 602.
[72] C.Y. Guo, Y.Y. Wang, K.Z. Xu, H.L. Zhu, P. Liu, Q.Z. Shi, S.M. Peng, Polyhedron 27 (2008) 3529–3536.

Ji-Fa Wang is currently pursuing his master's degree in the School of Chemical and Biological Engineering at Lanzhou Jiaotong University, China. He obtained his B.S. in the School of Materials Science and Engineering at Qilu University of Technology, China in 2018. E-mial: wjf19951008@126.com

Xin Xu is currently pursuing her master's degree in the School of Chemical and Biological Engineering at Lanzhou Jiaotong University, China. She obtained her bachelor's degree in the School of Chemistry and Chemical Engineering of Jining University, China, in 2018. E-mail: xxchemistry@163.com

Ruo-Nan Bian is currently pursuing her master's degree in the School of Chemical and Biological Engineering at Lanzhou Jiaotong University, China. She obtained her B.S.in the School of Chemical and Biological Engineering at Lanzhou Jiaotong University, China, in 2017. E-mail: brn0309@163.com

Wen-Kui Dong received his PhD degree in 1998 from Lanzhou University, China. He is a professor in the School of Chemical and Biological Engineering at Lanzhou Jiaotong University. His current research interests are focusing on the chemistry of functional supramolecular complexes, materials and new products, as well as processes and applications of environmental chemical engineering. E-mail: dongwk@126.com

Yu-Jie Ding received her PhD degree in 2013 from Nanjing University, China; She is an associate professor in College of Biochemical Engineering at Anhui Polytechnic University, her current research interesting is the synthesis and application of upconversion luminescence nanomaterials. E-mail: yujieding123@163.com